Conformational Changes in Photosystem II Supercomplexes upon Removal of Extrinsic Subunits†

Egbert J. Boekema,‡ Jan F. L. van Breemen,‡ Henny van Roon,§ and Jan P. Dekker*,§

Department of Biophysical Chemistry, Groningen Biomolecular Sciences and Biotechnology Institute, University of Groningen, Nijenborgh 4, 9747 AG Groningen, The Netherlands, and Faculty of Sciences, Division of Physics and Astronomy, Vrije Universiteit, De Boelelaan 1081, 1081 HV Amsterdam, The Netherlands

Received April 24, 2000; Revised Manuscript Received June 26, 2000

ABSTRACT: Photosystem II is a multisubunit pigment−protein complex embedded in the thylakoid membranes of chloroplasts. It consists of a large number of intrinsic membrane proteins involved in light-harvesting and electron-transfer processes and of a number of extrinsic proteins required to stabilize photosynthetic oxygen evolution. We studied the structure of dimeric supercomplexes of photosystem II and its associated light-harvesting antenna by electron microscopy and single-particle image analysis. Comparison of averaged projections from native complexes and complexes without extrinsic polypeptides indicates that the removal of 17 and 23 kDa extrinsic subunits induces a shift of about 1.2 nm in the position of the monomeric peripheral antenna protein CP29 toward the central part of the supercomplex. Removal of the 33 kDa extrinsic protein induces an inward shift of the strongly bound trimeric light-harvesting complex II (S-LHCII) of about 0.9 nm, and in addition destabilizes the monomer−monomer interactions in the central core dimer, leading to structural rearrangements of the core monomers. It is concluded that the extrinsic subunits keep the S-LHCII and CP29 subunits in proper positions at some distance from the central part of the photosystem II core dimer to ensure a directed transfer of excitation energy through the monomeric peripheral antenna proteins CP26 and CP29 and/or to maintain sequestered domains of inorganic cofactors required for oxygen evolution.

The photosynthetic apparatus of green plants consists of several membrane-bound complexes, of which photosystem II (PSII)[1] has the unique capacity to evolve oxygen from water. Three extrinsic proteins with apparent molecular masses of 33, 23, and 17 kDa are required for maximal rates of oxygen evolution at physiological inorganic cofactor concentrations (reviewed in refs *1*−*3*). The 33 kDa protein is encoded by the nuclear *psbO* gene, has a molecular mass of 26.5 kDa, and is in its solubilized form characterized by a high β-sheet structure content and a low α-helix structure content (*3*, *4*), which indicates that it has a rather rigid conformation. The content of β-sheet structure is probably even enhanced upon binding to PSII (*5*). The protein was suggested to have a prolonged ellipsoidal shape in solution (*6*) and to belong to the family of proteins that adopt a "natively unfolded" (*7*) or "molten globule" (*8*) structure. The stoichiometry of the 33 kDa protein is currently under debate. There is considerable biochemical evidence for the presence of two 33 kDa proteins per PSII reaction center (see, e.g., refs *3*, *9*, and *10*), but even the most recent structural work points to only one 33 kDa protein per PSII reaction center (*11*). The 33 kDa protein is generally termed the "manganese stabilizing protein" (MSP), because its removal leads to the release of manganese and a complete loss of the capacity of PSII to evolve oxygen at low chloride concentrations (*1*), and one of its main functions may be to maintain the chloride required for oxygen evolution in a "sequestered domain" close to the manganese cluster (*3*).

The other two proteins are less well characterized. The 23 kDa protein is encoded by the nuclear *psbP* gene and has a molecular mass of 20.2 kDa. Also, this protein is characterized by a high β-sheet structure content and a low α-helix structure content (*12*). The 17 kDa protein is encoded by the nuclear *psbQ* gene and has a molecular mass of 16.5 kDa. Both proteins occur most likely in a 1:1 stoichiometry with the PSII reaction center complex and bind less strongly to the PSII complex than the 33 kDa protein. Their functions may be to prevent the release of Ca^{2+} ions, to create a high-affinity binding site for Cl^- ions, and to stabilize the manganese cluster (*1*). Also, the 23 and 17 kDa proteins have been suggested to keep the chloride required for oxygen evolution in a sequestered domain close to the manganese cluster (*13*).

Recent progress in the analysis by electron microscopy of two-dimensional crystals of subcomplexes of PSII has revealed the position of the major core subunits at a resolution of slightly better than 1 nm. The most detailed map concerns a particle consisting of the D1, D2, and CP47 large subunits, but it does not contain the extrinsic subunits (*14*). Crystals from dimeric core complexes contain in

† This research was supported by the Netherlands Foundation for Scientific Research (NWO) via the Foundation for Life and Earth Sciences (ALW).

* To whom correspondence should be addressed. Telephone: +31 20 4447931. Fax: +31 20 4447999. E-mail: dekker@nat.vu.nl.

‡ University of Groningen.

§ Vrije Universiteit Amsterdam.

[1] Abbreviations: α-DM, *n*-dodecyl α-D-maltoside; C, monomeric PSII core complex; Chl, chlorophyll; EM, electron microscopy; L, loosely bound trimeric LHCII; LHCII, light-harvesting complex II; M, moderately bound trimeric LHCII; MSP, manganese stabilizing protein; PSI, photosystem I; PSII, photosystem II; S, strongly bound trimeric LHCII; X, trimeric LHCII not bound to the PSII core complex.

10.1021/bi0009183 CCC: $19.00
Published on Web 09/27/2000

addition CP43 and the 33 kDa protein (*15*, *16*). A projection map at 0.9 nm reveals at least 29 different transmembrane α-helices (*16*), but a complete three-dimensional (3D) structure at the same resolution has not yet been reported. In contrast to the two-dimensionally crystallized smaller particles, the larger PSII−LHCII supercomplexes also contain the 23 and 17 kDa extrinsic subunits (*17*), although the latter was only clearly demonstrated in the most recent work (*11*). In this work, a 3D map of the photosystem II supercomplex was obtained from single-particle projections in vitrified ice, in which the overall shape of the protrusions from the extrinsic subunits was well preserved. These protrusions consist of a tetrameric structure of four separated and rather spherical densities on top of a dimeric PSII−LHCII supercomplex. It was suggested that the two most central densities locate the 33 kDa protein and that the two other, slightly larger densities locate the 23 and 17 kDa extrinsic subunits (*11*), in line with earlier work based on electron microscopy using negatively stained specimens (*17*). The tetrameric structure clearly resembles the structures observed previously in freeze-etching studies of intact thylakoid membranes (see, e.g., ref *18*), suggesting that the structures observed in ref *11* represent the native organization of the PSII extrinsic subunits.

Biochemical (*19*−*21*) and ultrastructural (*22*−*25*) work on the PSII−LHCII supercomplexes has indicated that the most common PSII−LHCII supercomplex [called C_2S_2 in our nomenclature (*23*)] contains two symmetry-related structures, each consisting of at least one trimeric LHCII complex, one monomeric CP26 protein, and one monomeric CP29 protein. The CP26 protein was suggested to be closely associated with the CP43 core antenna protein, while CP29 probably is located close to CP47 (*20*). The PSII−LHCII supercomplexes were shown to be rather severely depleted in the very hydrophobic PsbS protein (*19*−*21*), which recently gained increased attention because of its prominent role in the physiologically important process of non-photochemical quenching (*26*), and may therefore not contain this protein. These complexes, however, may contain the recently discovered 6.6 kDa LhbA protein, which probably contains two transmembrane α-helices and which was shown to be associated with CP26 (*27*).

Despite the improved knowledge of the structural organization of the PSII core complex and of the location of the extrinsic proteins involved in oxygen evolution, little is known about the influence of the extrinsic subunits on the overall supramolecular organization of PSII. Freeze-etching studies of polypeptide-depleted PSII membranes (*18*, *28*) indicated that the removal of the 33, 23, and 17 kDa proteins by Tris washing changed the four-lobed structure into a two-lobed structure in which the two halves of the dimer are clearly separated. Details of the organization of PSII after Tris washing could, however, not be given because of the limited resolution of the freeze-etching technique. In previous work on the extrinsic subunits of PSII (*17*), it was noticed that the top-view projections of negatively stained PSII−LHCII supercomplexes with retained 23 kDa protein not only differed at positions assigned to the removed subunit but also had a slightly different overall shape. An acceptable explanation of this phenomenon could not be given at that time.

To investigate in detail in which respect the overall structure of the PSII−LHCII supercomplex depends on the presence of the extrinsic subunits, we present in this paper a structural study of PSII−LHCII supercomplexes obtained after a partial solubilization with the mild detergent *n*-dodecyl α-D-maltoside of PSII membranes depleted of the extrinsic polypeptides by standard salt or Tris washing procedures. The results demonstrate that the removal of the 23 and 17 kDa proteins induces changes in the positions of the peripheral antenna proteins and that the removal of the 33 kDa extrinsic protein induces additional changes in the positions of the peripheral antenna proteins and in addition destabilizes the dimeric structure of PSII.

MATERIALS AND METHODS

Sample Preparation. PSII membranes were isolated from freshly prepared spinach thylakoid membranes as described previously (*29*). The membranes were washed either with 2 M NaCl at pH 6.0 as described in ref *30* to remove the 23 and 17 kDa proteins or with 0.8 M Tris-HCl at pH 8.3 as described in ref *31* to remove all three extrinsic polypeptides. The membranes were resuspended and washed either in a buffer containing 20 mM BisTris (pH 6.5) and 5 mM $MgCl_2$ or in the same buffer without 5 mM $MgCl_2$ and were not frozen until they were used. For the preparation of PSII−LHCII supercomplexes, the methods reported in ref *24* were followed. In short, the oxygen-evolving or polypeptide-depleted PSII membranes were (at a final chlorophyll concentration of 1.9 mg/mL) partially solubilized with *n*-dodecyl α-D-maltoside (α-DM final concentration of 1.2%) in the above-mentioned buffer with or without $MgCl_2$, centrifuged to remove unsolubilized material, partially purified by gel filtration chromatography using a Superdex 200 HR 10/30 column (Pharmacia), and immediately prepared for electron microscopy as described in ref *24*.

Biochemical Characterization. Sucrose density gradient centrifugation was performed according to the method described in ref *25*. SDS−PAGE was performed on a 12% acrylamide gel according to the method of Schägger and von Jagow (*32*).

Electron Microscopy. Transmission electron microscopy was performed with a Philips CM10 electron microscope at 52000× magnification. Negatively stained specimens were prepared with a 2% solution of uranyl acetate on glow-discharged plain carbon-coated copper grids as described in ref *24* by diluting the samples 2−10-fold with buffer and 0.03% α-DM. Glow-discharged grids usually force molecules to attach with their flat sides on the film, thus preventing side views (*23*). From negatives with images of supercomplexes obtained from unstacked (without $MgCl_2$) salt-washed membranes, stacked (with $MgCl_2$) salt-washed membranes, unstacked Tris-treated membranes, and stacked Tris-treated membranes, we selected 3643, 180, 3009, and 4070 projections, respectively, with a window size of 96 pixels × 96 pixels, comparable to 46.6 nm × 46.6 nm.

Image Analysis. Image analysis was carried out with IMAGIC software (*33*). The projections were analyzed following an aperiodic (single particle) procedure, including repeated cycles of alignment procedures (*33*) and treatment by multivariate statistical analysis (*34*) and classification (*35*).

RESULTS

Sample Preparation. In previous reports, we have analyzed the association of PSII and its peripheral light-harvesting

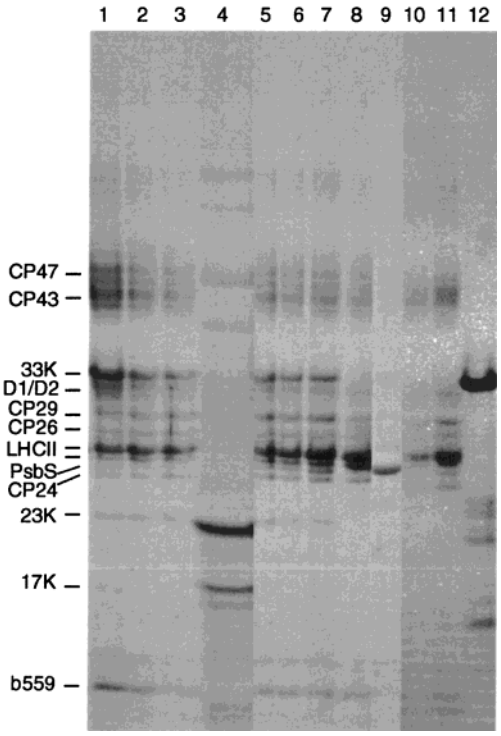

FIGURE 1: Identification by SDS−PAGE of polypeptides of PSII−LHCII supercomplexes purified by sucrose density gradient centrifugation. Lanes 1−3 and 5−7 show the polypeptide composition of complexes of increasing size obtained from α-DM-solubilized oxygen-evolving PSII membranes, and reveal a relative increase in the level of LHCII components compared to PSII core components in the larger fractions. Lane 4 shows the 23 and 17 kDa proteins released by the salt treatment of the membranes. Lane 8 shows Tris-washed PSII membranes, while lane 9 shows a partially purified PsbS protein. Lanes 10 and 11 show the polypeptide composition of two complexes of increasing size obtained from α-DM-solubilized Tris-washed PSII membranes. In lanes 8, 10, and 11, no traces of the 33 and 23 kDa extrinsic proteins can be seen. Lane 12 shows a partially purified 33 kDa protein. The gel was stained with Coomassie Brilliant Blue. On the left side of the gel, the positions of most of the PSII proteins are depicted. Lanes 10−12 were obtained from a different but identically run gel.

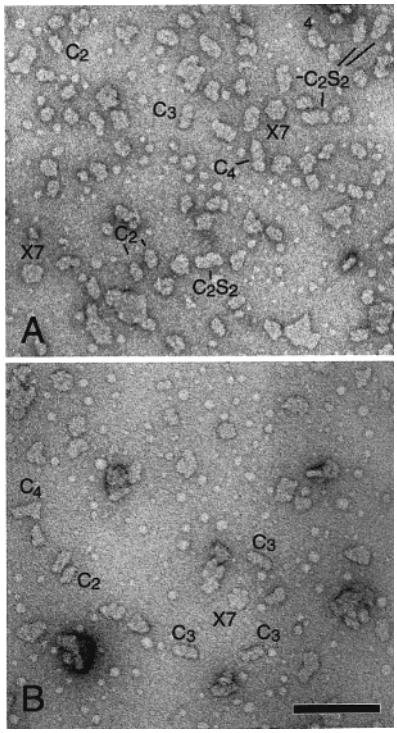

FIGURE 2: Electron micrographs of PSII complexes obtained from chromatographically purified unstacked (A) and stacked (B) α-DM-solubilized Tris-washed PSII membranes, negatively stained with uranyl acetate. C_2−C_4 denote dimeric, trimeric, and tetrameric PSII core complexes, respectively; C_2S_2 denotes the main PSII−LHCII supercomplex with two strongly bound trimeric LHCII complexes, and X_7 represents the heptameric association of trimeric LHCII, the so-called icosienamer. The scale bar is 100 nm long.

antenna by solubilizing PSII membranes prepared with Triton X-100 (*29*) with small amounts of the very mild detergent α-DM (*23*−*25*). During the course of the solubilization experiments with salt- or Tris-washed PSII membranes, however, it appeared that solubilization conditions similar to those used for native, oxygen-evolving PSII membranes resulted in many cases in a very poor solubilization of the membranes. The solubilization yield varied considerably from batch to batch (from about 0 to 15% on a chlorophyll basis), but was always much lower than with oxygen-evolving PSII membranes (∼50%). The solubilization yield could, however, be increased by omitting the divalent cations from the solubilization buffer. This can be explained by the idea that the presence of divalent cations induces a very tight stacking of the pair of membranes, on which the poor detergent α-DM cannot perform its solubilizing actions, whereas the absence of divalent cations induces a looser type of interaction between the two membranes, between which the detergent can now penetrate and solubilize the particles. In the following, we will refer to the membranes prepared in the presence and absence of 5 mM $MgCl_2$ as "stacked" and "unstacked", respectively.

To show whether the solubilization of the Tris-washed PSII membranes really resulted in supercomplexes without the extrinsic 33 kDa protein, we determined the polypeptide composition of native and Tris-treated supercomplexes purified on a sucrose density gradient. Figure 1 shows that the isolated Tris-treated PSII−LHCII supercomplexes indeed lack the extrinsic proteins, but that all other proteins are present. This result excludes the possibility that the isolated supercomplexes arise from a small fraction of PSII in which the 33 kDa protein has resisted the extraction. Figure 1 also indicates that in the smallest PSII−LHCII complexes from oxygen-evolving membranes (lanes 1−3) the PsbS protein is rather strongly depleted (the staining intensity is far below that of the CP29 and CP26 proteins), in agreement with earlier results (*19*−*21*). The larger complexes in lanes 5−7, however, show not only an increased LHCII content but also an increased PsbS protein content, suggesting that this protein could be bound to PSII in associations larger than the "standard" C_2S_2 PSII−LHCII supercomplex.

Electron Microscopy. Inspection of EM images of chromatographically purified complexes, obtained from salt-washed or Tris-washed and α-DM-solubilized PSII membranes, revealed the presence of several different types of projections (Figure 2). One main type could be easily attributed to the rectangular-shaped C_2S_2 PSII−LHCII supercomplex (*25*), and another type was the LHCII icosienamer (X_7), which was structurally characterized in an earlier report (*31*). Also, C_2S PSII−LHCII supercomplexes and C_2 PSII core complexes were observed. Besides these particles, which have already been studied extensively (see, e.g., ref

Table 1: Numbers of Assigned PSII−LHCII Supercomplexes, Megacomplexes, Trimeric and Tetrameric PSII Core Complexes, and Icosienamers (X_7) after Five Different Types of Treatment[a]

complex	native	salt-s	salt-u	Tris-s	Tris-u
total assigned	12755	68	1386	1285	2177
C_2S_2	9000	32	1202	279	1896
C_2S_2M	1860	0	11	7	5
$C_2S_2M_2$	120	0	0	0	0
C_2S_2L	85	2	11	3	19
C_2S_2ML	85	0	0	0	0
mega-I	360	0	0	0	12
mega-II	170	0	0	0	1
mega-III	39	0	0	0	0
X_7	100	2	14	139	206
C_4	4	32	148	387	19
C_3	0	ND	ND	470	19

[a] The starting materials were untreated membranes [native (from ref *25*)], stacked salt-washed membranes (salt-s), unstacked salt-washed membranes (salt-u), stacked Tris-washed membranes (Tris-s), and unstacked Tris-washed membranes (Tris-u).

Table 2: Relative Occurrence (in %) of the Various Trimeric and Monomeric LHCII Complexes in Super- and Megacomplexes, as Well as the Relative Occurrence of Trimeric LHCII in Icosienamers (X_7) and of PSII Core Complexes in Tetrameric Core Complexes (C_4) Compared to the Number of S Trimers[a]

complex	native	salt	Tris
total S	≡100	≡100	≡100
total M	16.5	0.9	1.5
total L	0.7	1.1	1.0
total CP29	100	99.5	93.9
total CP26	81.9	42.7	67.6
total CP24	16.5	0.9	1.5
total X in X_7	2.8	3.9	54.0
total C in C_4	0.1	28.6	36.1

[a] The numbers of LHCII trimers at the S-position in super- and megacomplexes were fixed to 100%. For the salt and Tris data, the sets obtained from unstacked and stacked membranes were merged.

22), two novel rod-like particles were present. These appeared to be C_2 core complexes to which an additional PSII core monomer or an additional PSII core dimer is associated on the short side. We will abbreviate these complexes as "C_3" and "C_4", respectively. We note that only very few complexes were lying on their side, which is probably caused by the use of glow-discharged grids (*23*).

The numbers of the different complexes were quite variable (Tables 1 and 2). The C_3 and C_4 rods were predominantly present in the samples derived from the stacked salt-washed or Tris-washed membranes, whereas the C_2S_2 supercomplexes dominated in the samples prepared from the unstacked salt-washed or Tris-washed membranes. The relative occurrence of the icosienamers, on the other hand, did not depend very much on the stacked or unstacked starting material, but on the Tris-washing pretreatment (Table 2).

Image Analysis. For a detailed comparison, about 11 000 extracted top-view particle projections from the salt- and Tris-treated samples were subjected to image analysis. After repeated multivariate statistical analysis and classification, on average about 44% of the projections were found to be interpretable. The lowest number of such projections was present in the data set obtained from Tris-washed, stacked membranes, where we noticed many relatively small fragments. Image analysis of the side views was not attempted, because the numbers of the particles were too low and the heterogeneity (PSII−LHCII supercomplexes, icosienamers, and trimeric and tetrameric PSII core complexes) was too large to perform a reliable statistical analysis.

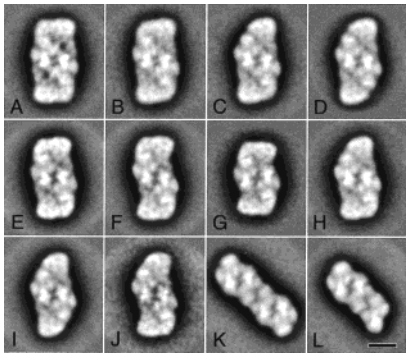

FIGURE 3: Results of multivariate statistical analysis and classification of top-view projections of PSII complexes isolated from salt-washed and Tris-washed PSII membranes. Average 29 projections of (A) 260 native, untreated C_2S_2 supercomplexes, obtained from ref *23*, (B) 175 salt-washed C_2S_2 supercomplexes, (C) 350 salt-washed C_2S_2 supercomplexes lacking one CP26 area, (D) 300 salt-washed C_2S_2 supercomplexes lacking two CP26 areas, (E) 300 type 1 Tris-washed C_2S_2 supercomplexes, (F) 300 type 2 Tris-washed C_2S_2 supercomplexes, (G) 116 type 2 Tris-washed C_2S_2 supercomplexes, (H) 300 type 1 Tris-washed C_2S_2 supercomplexes lacking one CP26 area, (I) 300 type 1 Tris-washed C_2S_2 supercomplexes lacking two CP26 areas, (J) 121 type 2 Tris-washed C_2S_2 supercomplexes lacking one CP26 area, (K) 200 Tris-washed C_4 supercomplexes, and (L) 400 Tris-washed C_3 supercomplexes. After analysis had been completed, 2-fold rotational symmetry was imposed on the images of panels A, B, D−G, I, and K. The scale bar is 10 nm long.

The final results of the multivariate statistical analysis and classification of top-view projections of PSII complexes isolated from salt-washed and Tris-washed grana membranes are presented in Figure 3. Average projections of salt-washed C_2S_2 supercomplexes (Figure 3B) and salt-washed C_2S_2 supercomplexes lacking one or two CP26 areas (Figure 3C,D) do not differ strongly from the native C_2S_2 supercomplex (Figure 3A). The most obvious differences are given by the stain-filled regions between the PSII core parts and the peripheral antenna, which are considerably more prominent in the native samples than in the salt-washed samples (see also refs *23*−*25* and Figure 4A−C).

Some supercomplexes from the Tris-treated samples exhibit an altered overall shape, and in fact, three different types were found by classification. The type 1 supercomplex (Figure 3E) has about the same rectangular shape as the supercomplex obtained from salt-washed membranes (Figure 3B). The main differences between the images of the Tris-washed type 1 supercomplex (see also Figure 4D) and the salt-washed supercomplex (Figure 4C) are the amount of stain in the central part of the dimer, which is considerably increased after Tris treatment. Also, in Tris-washed dimeric PSII core complexes from spinach and *Synechococcus elongatus*, the amount of stain in the central part of the dimer was increased after removal of the 33 kDa protein (*22*). In the type 2 C_2S_2 supercomplex, the rectangular shape is modified into a kind of elongated, S-shaped configuration (Figure 3F), whereas in the type 3 complex, the shape is modified into a considerably shortened, S-shaped configuration (Figure 3G). As with the salt-treated supercomplexes, a substantial number of type 1 and type 2 supercomplexes lack one or two CP26 subunits (Figure 3H−J), but apart from

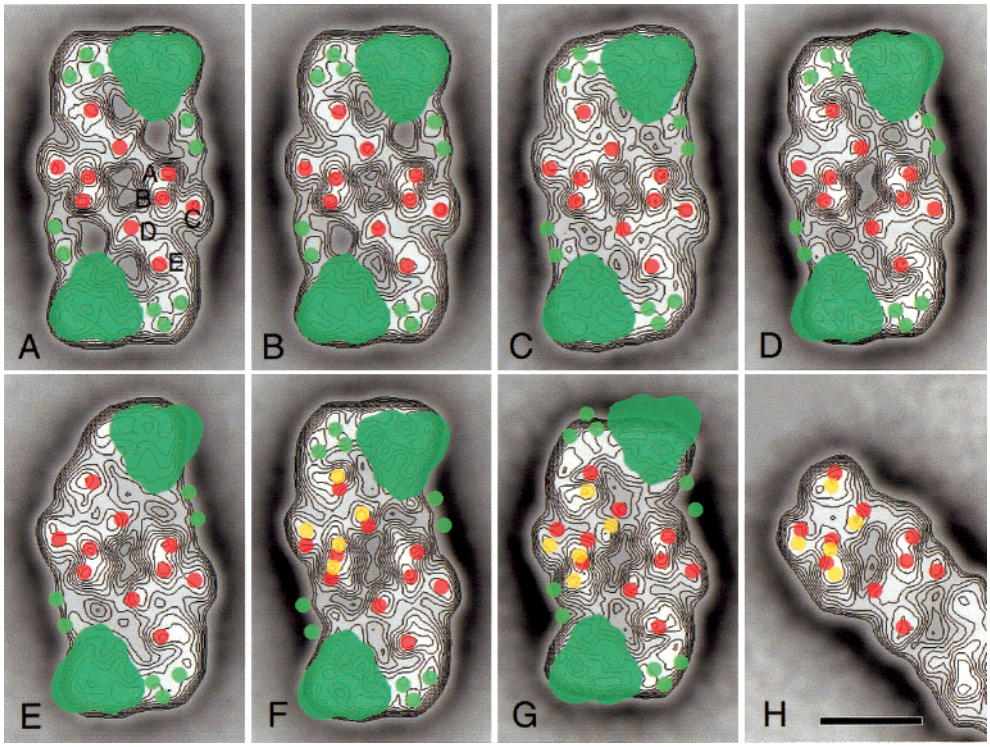

FIGURE 4: Demonstration of the changes in the position of peripheral antenna and core proteins within C_2S_2 supercomplexes after salt or Tris washing. (A) The contoured version of Figure 3A [representing C_2S_2 supercomplexes isolated without any purification (*23*)], in which the S-type LHCII trimer is indicated by a full green triangle, CP29 by two green dots, CP26 by three green dots, and the PSII core part by five red dots. The positions of stain-excluding densities in the PSII core part were designated A−E as done previously (*17*). (B) The sum of 600 chromatographically purified, untreated C_2S_2 supercomplexes [reproduced from (*24*)], with the green and red overlays of panel A superimposed. (C) The salt-washed complete C_2S_2 supercomplex from Figure 3B with the overlays of panel A superimposed. (D) The type 1 Tris-washed complete C_2S_2 supercomplex from Figure 3E with the overlays of panel A superimposed. (E) The type 1 Tris-washed C_2S_2 supercomplex without one CP26 area from Figure 3H with the overlays of panel A superimposed. (F) The type 2 Tris-washed complete C_2S_2 supercomplex from Figure 3F with the overlays of panel A superimposed. The yellow dots represent the densities in the left PSII core monomer and indicate an upward shift of the left monomer. (G) The type 3 Tris-washed complete C_2S_2 supercomplex from Figure 3G with the overlays of panel A superimposed. The yellow dots represent the densities in the left PSII core monomer and indicate a downward shift of the left monomer. (H) The Tris-washed C_4 PSII core complex from Figure 3K. The positions of red and yellow dots indicate a shift similar to that shown in panel G. Note that since the number of projections used for the calculations for panels C and G was limited, some particles lacking the CP26 tip were included in the final sums, resulting in a slight overall reduction in this area. Otherwise, this area does not seem to be substantially changed in position, in contrast to CP29. The scale bar is 10 nm long.

these features, the supercomplexes appear not to be essentially different. In particular, very similar differences are observed between the type 1 and type 2 "complete" supercomplexes (Figure 3E,F) and the type 1 and type 2 supercomplexes with one empty CP26 binding site (Figure 3H,J). This indicates that the observed types of variation have not been induced by the image analysis procedures, because the sets of complete and (partially) CP26-depleted supercomplexes were independently processed.

The analysis of the two rodlike projections from the Tris-treated samples shows that the average projection of the larger one, the C_4 complex, has a two-fold rotational symmetry and thus is composed of two identical C_2 dimers (Figure 3K). In the C_3 complex, one of the core monomers is lacking, but otherwise, the particles are identically composed (Figure 3L). The C_4 and C_3 complexes obtained from the salt-washed membranes have a very similar shape (not shown).

To find out in which respect the new types of projections are unique for polypeptide-depleted PSII supercomplexes, we re-examined the complete data set of 16 600 complexes obtained from native, oxygen-evolving PSII membranes (*25*) with the averages of the shortened PSII−LHCII supercomplex (Figure 3G) and the C_3 and C_4 complexes (Figure 3K,L) as references. These particles were not observed previously by the automatic classification procedures. The re-examination revealed fewer than five particles of each of the three groups, whereas there were at least 100 of each in the smaller data set derived from the Tris-washed PSII membranes, and also at least 100 C_3 and C_4 complexes in the data set derived from the salt-washed PSII membranes (see also Table 1 and the legend of Figure 3). The shortened C_2S_2 supercomplexes, however, were not present in significant numbers in the data set from the salt-washed material. These results indicate that the shortened C_2S_2 supercomplexes (Figure 3G) represent a unique structure specifically induced by the Tris treatment and that the occurrence of the C_3 and C_4 complexes is induced by the salt or Tris treatment.

Conformational Differences between Projections. A close comparison of the different types of particle projections, obtained after salt or Tris washing, with native supercomplexes shows changes in intensities of masses in the core part of PSII, as well as significant rearrangements in the peripheral antenna (Figure 4). The rearrangements mostly concern the CP29 subunit (indicated by the pair of green dots in Figure 4) and the S-LHCII trimer (the triangular green structure in Figure 4). In the salt-washed particle (Figure 4C), there are inward shifts of CP29 and the S-LHCII trimer

of about 1.2 and 0.3 nm, respectively, indicating that salt washing mainly affects the position of CP29. Very similar shifts (within 0.2 nm) were observed in the independently processed images of projections with one CP26 tip (not shown), suggesting that the observed variation is reproducible. The shifts coincide with a decrease in the amount of stain near mass "D" (see Figure 4A). In the type 1 Tris-washed particle (Figure 4D), there are similarly directed shifts of CP29 and the S-LHCII trimer of 1.3 and 0.9 nm, respectively, suggesting that the additional effect of removing the 33 kDa protein affects mainly the S-LHCII trimer. The positions of the masses in the core parts of the salt-washed particles (Figure 4C) and the type 1 Tris-washed particles (Figure 4D) are not significantly displaced.

The images of the type 2 and type 3 Tris-washed particles and the C_4 rods show a more complicated situation. In the type 2 particles, the CP29 subunits have moved in further (about 2.8 nm, Figure 4E,F), but also within the core part, several densities have changed significantly in position. Since densities A−E belonging to one core monomer all show the same kind of shift (yellow masses, Figure 4F), it can be concluded that the complete left core monomer underwent an upward shift of about 1.2 nm, including the upper LHCII trimer and CP26. This rearrangement of the core monomers also leads to a reduction in the size of the central stain-filled cavity. In the type 3 particles, even stronger changes have taken place (Figure 4G). The position of the LHCII trimers with respect to the core part indicates that in these particles the CP29 proteins have been released (discussed in more detail below). The absence of CP29 now leads to a downward shift of 2 nm of the left core monomer. A similarly directed but slightly smaller shift (1.5 nm) has occurred in the C_4 core rods (Figure 4H), which do not contain peripheral LHCII antenna proteins.

Difference Mapping. The effect of salt and Tris washing on the central core part area of the supercomplex (densities A, B, D, and E in Figure 4A) has been further evaluated by generating difference maps. The difference maps between the native supercomplex of Figure 4A and the three independently averaged salt-washed particles from Figure 3B−D are similar and show some changes in the density D region (Figure 5A−C). Similar changes are visible in the difference map from the type 1 Tris-washed supercomplex (Figure 5E), but in addition, this image indicates a substantial reduction in the mass in the central region of the dimeric supercomplex. The type 2 complexes exhibit a similar pattern (not shown), and the type 3 particles also exhibit a small reduction in mass at the position of density B (Figure 5F). This mass is also reduced in other difference images (Figure 5G, and those of the Tris-washed C_3 and C_4 PSII core complexes, not shown).

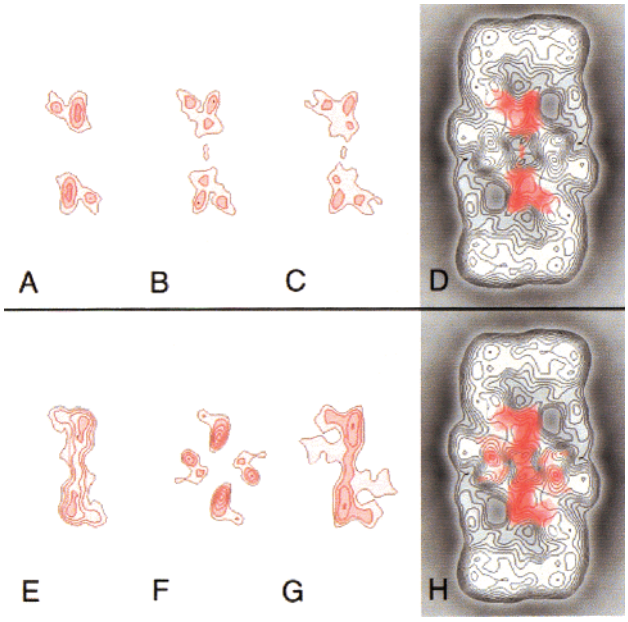

FIGURE 5: Difference mapping of C_2S_2 supercomplexes. (A−C) Effect of salt washing. Difference images in the PSII core parts between panels A and B−D of Figure 3, respectively. (D) Images of panels A−C superimposed on the native C_2S_2 supercomplex. (E−G) Effect of Tris washing. Difference images between panels A and E, G, and I of Figure 3, respectively. (H) Images of E−G superimposed on the native C_2S_2 supercomplex. Note that the levels in panels A−C and E−G have the same equidistancy as in panels D and H, indicating a ≤40% local difference.

DISCUSSION

Supercomplexes without the 33 kDa Extrinsic Subunit. Supercomplexes of PSII and LHCII have been isolated and biochemically and structurally characterized previously (see, e.g., ref *22*), but, as yet, not after a pretreatment of the PSII membranes to remove the extrinsic 33 kDa protein. Compared to the previously characterized supercomplexes with the retained 33 kDa protein, the 33 kDa-depleted supercomplexes exhibit the unique feature that exists in three different types, of which types 2 and 3 show a markedly different structure of the central PSII core dimer. In the type 2 complex, the left part of the supercomplex is laterally shifted in the upward direction, whereas in the type 3 complex, this part is laterally shifted in the downward direction (Figure 4). In both cases, the shifts are considerable (up to about 2 nm).

These changes point to a destabilization of the PSII core−core interactions upon removal of the 33 kDa protein. Also, in PSII from the cyanobacterium *S. elongatus*, it was noticed that the dimeric PSII core complex was unstable after Tris treatment (*36*), suggesting that the stabilizing effect is a general property of the 33 kDa protein. It is not clear by which mechanism the dimeric PSII core structure is stabilized by the 33 kDa protein. Recent evidence has indicated that a small, membrane-bound subunit is present in the central part of the PSII core dimer (*16*), and also that certain lipids play an essential role in the formation and/or stabilization of the dimers (*37*). It is, however, not very likely that the small protein (indicated in yellow in Figure 6) and the lipids are absent in our supercomplexes, because the Tris treatment is not expected to remove membrane-bound subunits or other hydrophobic components. In our opinion, the possibility should be seriously considered that the 33 kDa protein partially covers the central region of the PSII core dimer and perhaps even extends to the adjacent monomer, and thus prevents detergents to act on the central region of the PSII core dimer. This possibility would give a straightforward explanation for the more pronounced staining of the central part of the PSII core structure in the type 1 Tris-treated supercomplex.

We note that our very short and mild detergent treatment using α-DM may have been a prerequisite for retaining the

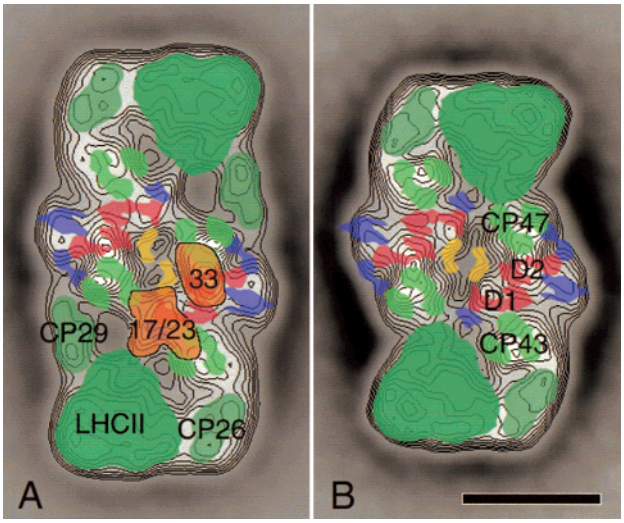

FIGURE 6: Positions of subunits in the native C_2S_2 supercomplex (A) and the Tris-washed type 3 C_2S_2 supercomplex (B). The positions of the 17, 23, and 33 kDa subunits (from panels B and F of Figure 5) have been indicated in panel A in orange. The densities of the PSII core dimer, calculated to a resolution of 0.9 nm, are presented in red (D1/D2), green (CP47 and CP43), and blue and yellow (unassigned densities) [adapted from Hankamer et al. (*16*)]. Modeling of the same densities in the type 3 Tris-washed supercomplex indicates a removal of both CP29 monomers, a shift of the core densities with respect to each other and an inward shift of the LHCII trimer. The scale bar is 10 nm long.

destabilized dimeric association in the 33 kDa-depleted complexes and that the type 3 supercomplexes obtained from the Tris-treated PSII membranes are the first supercomplexes in which the monomeric antenna protein CP29 is not present (Figure 6B). In supercomplexes obtained from native PSII membranes, no empty CP29 binding sites have been found, in clear contrast to CP26, which was explained by a successive accumulation of CP29, S-LHCII, and CP26 to the dimeric PSII core complex during biogenesis (*25*). The absence of CP29 in the type 3 supercomplexes is most likely caused by the destabilized association of the central core dimer. The S-LHCII and CP26 complexes in the lower half of the complex are almost exclusively bound to the right half of the PSII core dimer (Figure 6A), and when the left half moves downward as a result of the destabilization, the CP29 complexes are forced into a position at the outside of the complex, where they are very vulnerable to a detergent-induced separation from the supercomplex.

Supercomplexes without the 23 and 17 kDa Extrinsic Subunits. PSII−LHCII supercomplexes without the 23 and 17 kDa proteins are not new, and in fact, the first published structure of such a complex (*22*) lacked these extrinsic subunits. In subsequent work (*17*), the differences between these 23 kDa free and glycine-betaine-stabilized, 23 kDa-retaining supercomplexes were analyzed by EM using negatively stained specimens, and it was concluded that the 23 kDa protein is located near position D (Figure 4), which was later confirmed by a 3D reconstruction using frozen and hydrated specimens (*11*).

The results described in this paper clearly point to a rearrangement of peripheral antenna subunits upon removal of the 23 and 17 kDa extrinsic proteins. In particular, the CP29 protein moves in the direction of the core complex by about 1.2 nm upon removal of these proteins. There is a slight displacement of the S-LHCII trimer; otherwise, there are no

Table 3: Total Area (in nm^2) of Top-View Projections of PSII−LHCII Supercomplexes

complex	complete	−1 × 26/29	−2 × 26/29
native C_2S_2	480	ND[a]	ND
salt C_2S_2	460	431	422
Tris type 1 C_2S_2	431	417	380
Tris type 2 C_2S_2	426	394	ND
Tris type 3 C_2S_2	−	−	388

[a] ND, not determined.

significant shifts of density positions, and the dimeric structure of the PSII core complex remains basically unchanged (Figure 4D). There are, however, a number of changes of density near position D (discussed in more detail below). We conclude that after removal of the protein(s) at density D, the CP29 monomer has space to move in the direction of the core complex, and thus gives rise to a reduction in the area of the supercomplex, which we estimate to be about 20 nm^2 for the complete, dimeric complex (Table 3).

An estimation of the sizes of the Tris-washed complexes indicates that the Tris washing gives rise to an additional shrinking of the supercomplexes (compared to the salt-washed particles) by, again, about 20 nm^2 (Table 3). The data shown in Figure 4 suggest that the additional shrinking upon removal of the 33 kDa extrinsic protein is mainly caused by a shift of the S-LHCII trimer in the direction of the core complex. At the same time, the overall shape of the supercomplexes changes from a rectangular view for the native complexes into a more and more S-shaped configuration upon increasing the "harshness" of the treatment (Figure 4). The first published supercomplex projection maps (*17*, *22*) support this view, since they all show an S-shaped configuration, indicating the detrimental effect of freezing and prolonged storage on the fine structure of the isolated supercomplex samples.

Figure 4 also suggests that some loss of the extrinsic proteins in combination with the shift is easily induced. The independently averaged projections (Figure 4A,B) from the C_2S_2 supercomplex isolated without any purification step (*23*), or by a single gel filtration chromatography step (*24*), exhibit almost identical positions of all densities. However, a 0.2 nm inward shift of the CP29 area can be noticed in the samples purified by gel filtration (Figure 4B). This might look insignificant, but it falls within the overall picture, in which the shift increases from milder to harsher treatment. It can thus be expected that any loss of extrinsic subunits results in a small average shift of CP29.

Particle Distribution. The ratios of the various types of complexes, analyzed by electron microscopy after a mild solubilization of oxygen-evolving PSII membranes with α-DM, have been presented previously (*25*). The results described in this contribution indicate that a pretreatment of the PSII membranes by salt or Tris washing induces substantial changes in the relative and absolute numbers of these complexes (Tables 1 and 2). There is a strong decrease in the numbers of associated M-type LHCII trimers, whereas no substantial change is seen in the association of the L-type trimers. We speculate that the reduction in the numbers of associated M-type trimers is caused by the lateral shift of the CP29 subunit, which is located very close to the M-type trimer in the native structure (*25*). In contrast, the numbers

of the L-type LHCII trimer, which are low anyway, do not disproportionally decrease with the salt and Tris treatment. This can be explained by the fact that this trimer binds directly to CP43 and CP26, which do not undergo strong positional changes upon the removal of extrinsic subunits (Figure 4).

Trimeric and Tetrameric PSII Core Particles. There is also a strong increase in the amount of LHCII-free PSII core complexes (C_3 and C_4) upon salt or Tris washing (Tables 1 and 2), which can be explained by the idea that the structure of the peripheral antenna is not only more closely associated with the PSII core dimer after salt or Tris washing but also less stable and more vulnerable to detergent-induced dissociation. We note that trimeric and tetrameric PSII core particles from higher plants have not been isolated and characterized thus far. The C_4 particle belongs in fact to the category of "megacomplexes" (*24*, *25*), which also consist of four central PSII core units. The interaction between the two core dimers in the tetrameric PSII core complex differs from that in each of the three types of previously observed megacomplexes (*24*, *25*), in which the monomeric LHCII proteins, in particular CP26, play an important role in the association. Also, in C_4 particles isolated from the cyanobacterium *S. elongatus*, a different association was observed (*38*). However, an association of PSII core dimers on their short sides as in our C_3 and C_4 particles (Figure 3K,L) has also been observed in various two-dimensional crystals of PSII core dimers (*39*) and in a minor crystal form observed in grana membranes (E. J. Boekema et al., unpublished observations). This suggests that the manner of association as observed in our C_3 and C_4 particles could become prominent if the peripheral antenna is partially detached.

Positions of Extrinsic Subunits. In comparison to previous work, which was based on side views of negatively stained specimens (*17*) and a 3D reconstruction of frozen and hydrated specimens (*11*), this paper does not provide much new insight into the number and positions of the extrinsic subunits on the structure of the dimeric PSII core complex. The summarized results of our experiments (Figure 6A) basically confirm the assignments in ref *11*, in which the 23 and 17 kDa proteins are placed near position D (Figure 4A) and the 33 kDa protein is placed near position B. The lack of new insight into this matter is probably inherent to the applied technique (the analysis of top-view projections of negatively stained specimens), which is quite powerful in the detection of lateral shifts of certain complexes, but less powerful in the assignment of the various stain-excluding regions, because not only the protein densities but also the specific interaction of the stain with the protein determines the amount of signal (as in frozen and hydrated specimens). If, for instance, protein density would be the most important factor for the signal, the stain exclusion would be expected to be most prominent at position D, because here the protein protrudes maximally above the surface of the supercomplex (*11*). All our images, however, show maximal stain exclusion near position B, where CP47 and the 33 kDa protein are located.

We point out that this paper provides the largest set of projections obtained thus far from negatively stained PSII supercomplexes with attached or detached extrinsic subunits and that, given the sizes of the three types of extrinsic proteins, the differences between the various projections are in fact remarkably small. For instance, a study using negatively stained projections from various polypeptide-depleted trimeric PSI particles revealed much larger effects of the absence of extrinsic subunits (*40*). The most stain-excluding regions of the PSII supercomplexes are located at positions A and B, irrespective of the presence of the extrinsic subunits (Figure 3). This means that the specific features of this stain-excluding structure must be caused by the intrinsic membrane proteins, in particular CP47 (Figure 6). The absence of very clear features of the extrinsic proteins can possibly be explained by an aglobular shape, as suggested by Zubrzycki et al. (*6*). However, the extrinsic protrusions on the lumenal side of the complex do have a globular shape (*11*). This obvious inconsistency can perhaps be explained by assuming that the globular protrusions in ref *11* consist only partially of extrinsic subunits and that the large extrinsic loops of CP47 and/or CP43 also contribute to these globular protrusions.

An indication that the 33 kDa protein either does not have a globular shape or is present in two copies per PSII monomer is given by our finding that its absence influences both the dimeric organization of PSII (and thus has a direct effect on the PSII core−core interaction) and the association with the strongly bound trimeric LHCII complex. The distance from density B to the central part of the dimer is not very large (less than 4 nm), which easily explains the influence of the 33 kDa protein on the core−core interaction. However, the area covered by the globularly shaped mass attributed to the 33 kDa protein in ref *11* and Figure 6A seems not to be large enough to significantly influence the region between the PSII core and S-LHCII, since this is at least 6 nm away in another direction (Figure 6). An aglobular shape and/or the presence in two copies per PSII monomer would give a rather simple explanation for the effect of the 33 kDa protein on the association of the peripheral antenna. The effect of the 23 and/or 17 kDa protein on the association of the peripheral antenna, however, is easy to understand because the globular mass attributed to these proteins (*11*) exceeds the region of the PSII core dimer, and clearly extends to the CP29 and S-LHCII subunits (Figure 6A). The difference mapping shown in Figure 5 is in line with these ideas.

Implications of the Interaction of Extrinsic Subunits with LHCII. The data presented above firmly establish significant conformational changes in the PSII structure upon the removal of extrinsic subunits, and we conclude that in native PSII at least the 33 kDa extrinsic subunit acts to keep the S-type LHCII trimers at a fixed distance from the core complex. The modeling of Figure 6 indicates that in the type 3 complex the closest distance from the S-LHCII to CP43 has been reduced by about 0.8 nm and from S-LHCII to D1 by about 1.3 nm (Figure 6). This raises the question of why the S-type LHCII trimer is kept some distance from the PSII core complex. A very close association of S-LHCII and the PSII core complex is probably not necessary for efficient light harvesting, because the excitation energy can probably migrate very well via the CP29 and CP26 complexes to the CP47 and CP43 core antenna proteins of PSII, respectively. A directed route of energy flow through the monomeric antenna proteins can even be advantageous for regulatory purposes, because these proteins are very much able to bind zeaxanthin, which is generated from violaxanthin during the

xanthophyll cycle under high-light conditions (*41*). Binding of zeaxanthin was shown to reduce the fluorescence quantum yield to a much larger extent in the monomeric CP26 and CP29 proteins than in trimeric LHCIIb (*42*), suggesting that specific control of light-harvesting efficiency can be generated if the energy transfer proceeds predominantly through the monomeric LHCII proteins.

Another possible reason the S-type LHCII trimers and CP29 monomers have to be kept some distance from the central part of the PSII core complex may be given by the inorganic cofactor requirement for the oxygen-evolving process. A connection between the site of water oxidation and the peripheral antenna proteins has indeed been demonstrated (*43*), though the stoichiometry of the thylakoid-like proton release pattern in LHCII-depleted PSII core particles could be restored by the addition of glycerol (*44*). During S-state cycling, a chloride ion is transiently bound to the manganese cluster responsible for oxygen evolution (*45*), and both the 33 kDa protein (*3*) and the 23 and 17 kDa proteins (*13*) have been suggested to keep the chloride in a sequestered domain close to the manganese cluster. The latter proteins may also function to keep calcium ions close to the manganese cluster, because in the absence of the 23 and 17 kDa proteins the calcium requirement for oxygen evolution is greatly increased (*1*). The volume of the sequestered domain for chloride was estimated to be at most a few cubic nanometers (*13*), which is much smaller than the decreased volume of about 50 nm^3 caused by the removal of the 23 and 17 kDa proteins (the product of the decreased area of 10 nm^2 and a membrane thickness of 5 nm). It is, however, not at all necessary that the sequestered domain occupy the complete extra volume. It is also possible that the sequestered domain for inorganic cofactors influences not only the catalytic site of oxygen evolution near the reaction center but also the peripheral antenna. For instance, the CP29 protein was recently shown to have a Ca^{2+} binding site near the extrinsic loop between the B and C transmembrane helices (*46*). This binding site could play an important role in photoregulation.

ACKNOWLEDGMENT

We thank Dr. W. Keegstra for his help with image processing.

REFERENCES

1. Seidler, A. (1996) *Biochim. Biophys. Acta 1277*, 35−60.
2. Debus, R. J. (2000) *Metal Ions Biol. Syst. 37*, 657−711.
3. Bricker, T. M., and Frankel, L. K. (1998) *Photosynth. Res. 56*, 157−173.
4. De Las Rivas, J., and Heredia, P. (1999) *Photosynth. Res. 56*, 11−21.
5. Hutchison, R., Betts, S. D., Yocum, C. F., and Barry, B. A. (1998) *Biochemistry 37*, 5643−5653.
6. Zubrzycki, I. Z., Frankel, L. K., Russo, P. S., and Bricker, T. M. (1998) *Biochemistry 37*, 13553−13558.
7. Lydakis-Simantiris, N., Hutchison, R. S., Betts, S. D., Barry, B. A., and Yocum, C. F. (1999) *Biochemistry 38*, 404−414.
8. Shutova, T., Irrgang, K.-D., Klimov, V. V., and Renger, G. (2000) *FEBS Lett. 467*, 137−140.
9. Leuschner, C., and Bricker, T. M. (1996) *Biochemistry 35*, 4551−4557.
10. Betts, S. D., Ross, J. R., Pichersky, E., and Yocum, C. F. (1997) *Biochemistry 36*, 4047−4053.
11. Nield, J., Orlova, E. V., Morris, E. P., Gowen, B., van Heel, M., and Barber, J. (2000) *Nat. Struct. Biol. 7*, 44−47.
12. Zhang, H., Ishikawa, Y., Yamamoto, Y., and Carpentier, R. (1998) *FEBS Lett. 426*, 347−351.
13. Wincencjusz, H., Yocum, C. F., and van Gorkom, H. J. (1998) *Biochemistry 37*, 8595−8604.
14. Rhee, K.-H., Morris, E. P., Barber, J., and Kühlbrandt, W. (1998) *Nature 396*, 283−286.
15. Morris, E. P., Hankamer, B., Zheleva, D., Friso, G., and Barber, J. (1997) *Structure 5*, 837−849.
16. Hankamer, B., Morris, E. P., and Barber, J. (1999) *Nat. Struct. Biol. 6*, 560−564.
17. Boekema, E. J., Nield, J., Hankamer, B., and Barber, J. (1998) *Eur. J. Biochem. 252*, 268−276.
18. Seibert, M., DeWit, M., and Staehelin, L. A. (1987) *J. Cell Biol. 105*, 2257−2265.
19. Hankamer, B., Nield, J., Zheleva, D., Boekema, E., Jansson, S., and Barber, J. (1997) *Eur. J. Biochem. 243*, 422−429.
20. Harrer, R., Bassi, R., Testi, M. G., and Schäfer, C. (1998) *Eur. J. Biochem. 255*, 196−205.
21. Eshaghi, S., Andersson, B., and Barber, J. (1999) *FEBS Lett. 446*, 23−26.
22. Boekema, E. J., Hankamer, B., Bald, D., Kruip, J., Boonstra, A. F., Barber, J., and Rögner, M. (1995) *Proc. Natl. Acad. Sci. U.S.A. 92*, 175−179.
23. Boekema, E. J., van Roon, H., and Dekker, J. P. (1998) *FEBS Lett. 424*, 95−99.
24. Boekema, E. J., van Roon, H., Calkoen, F., Bassi, R., and Dekker, J. P. (1999) *Biochemistry 38*, 2233−2239.
25. Boekema, E. J., van Roon, H., van Breemen, J. F. L., and Dekker, J. P. (1999) *Eur. J. Biochem. 266*, 444−452.
26. Li, X.-P., Björkman, O., Shih, C., Grossman, A. R., Rosenquist, M., Jansson, S., and Niyogi, K. K. (2000) *Nature 403*, 391−395.
27. Ruf, S., Biehler, K., and Bock, R. (2000) *J. Cell Biol. 149*, 369−377.
28. Santini, C., Tidu, V., Tognon, G., Ghiretti Magaldi, A., and Bassi, R. (1994) *Eur. J. Biochem. 221*, 307−315.
29. Berthold, D. A., Babcock, G. T., and Yocum, C. F. (1981) *FEBS Lett. 134*, 231−234.
30. Ghanotakis, D. F., Babcock, G. T., and Yocum, C. F. (1984) *FEBS Lett. 167*, 127−130.
31. Dekker, J. P., van Roon, H., and Boekema, E. J. (1999) *FEBS Lett. 449*, 211−214.
32. Schägger, H., and von Jagow, G. (1987) *Anal. Biochem. 166*, 368−379.
33. Harauz, G., Boekema, E., and van Heel, M. (1988) *Methods Enzymol. 164*, 35−49.
34. Van Heel, M., and Frank, J. (1981) *Ultramicroscopy 6*, 187−194.
35. Van Heel, M. (1989) *Optik 82*, 114−126.
36. Dekker, J. P., Boekema, E. J., Witt, H. T., and Rögner, M. (1988) *Biochim. Biophys. Acta 936*, 307−318.
37. Kruse, O., Hankamer, B., Konczak, K., Gerle, C., Morris, E., Radunz, A., Schmid, G. H., and Barber, J. (2000) *J. Biol. Chem. 275*, 6509−6514.
38. Kuhl, H., Rögner, M., van Breemen, J. F. L., and Boekema, E. J. (1999) *Eur. J. Biochem. 266*, 453−459.
39. Lyon, M. K. (1998) *Biochim. Biophys. Acta 1364*, 403−419.
40. Kruip, J., Chitnis, P. R., Lagoutte, B., Rögner, M., and Boekema, E. J. (1997) *J. Biol. Chem. 272*, 17061−17069.
41. Horton, P., Ruban, A. V., and Walters, R. G. (1996) *Annu. Rev. Plant Physiol. Plant Mol. Biol. 47*, 655−694.
42. Wentworth, M., Ruban, A. V., and Horton, P. (2000) *FEBS Lett. 471*, 71−74.
43. Jahns, P., and Junge, W. (1993) *Photochem. Photobiol. 57*, 120−124.
44. Haumann, M., Hundelt, M., Jahns, P., Chroni, S., Bögershausen, O., Ghanotakis, D., and Junge, W. (1997) *FEBS Lett. 410*, 243−248.
45. Wincencjusz, H., van Gorkom, H. J., and Yocum, C. F. (1997) *Biochemistry 36*, 3663−3670.
46. Jegerschöld, C., Rutherford, A. W., Mattioli, T. A., Crimi, M., and Bassi, R. (2000) *J. Biol. Chem. 275*, 12781−12788.

BI0009183